A current perspective of the state-of-the-art in stress analysis

Akimitsu Nezu*, Hitomi Matsuzaka* and Ryouichi Yokoyama**

1. Introduction

This paper discusses recent methods in X-ray stress analysis. The authors have selected three examples thought to be the most practical from among the many X-ray stress measurement and analysis methods other than the conventional $\sin^2\psi$ method. The examples of analyses presented here are: (1) residual stress measurement using the multiple-hkl method, (2) residual stress measurement of samples with shear stress in the depth direction, and (3) residual stress measurement and line-broadening of diffraction in samples with fibre texture using the crystallite strain analysis method.

2. X-ray residual stress measurement using the multiple-hkl method

2.1. Thin-film X-ray diffraction measurement using the grazing-angle incidence method

In surface treatment using hard ceramic films, the materials used have outstanding properties such as low friction, and wear, heat, and corrosion resistance, and thus such films are widely used in cutting tools, machinery parts, dies, decorations, magnetic recording media and other applications. Typical examples of ceramic films include nitrides such as TiN, TiAlN, TiC, AlN and CrN. Among these, TiN films can be used at high temperatures while maintaining high hardness and good adhesion with steel and cemented carbide. As a result TiN is used in a wide range of fields as a protective coating material. The PVD (Physical Vapor Deposition) and CVD (Chemical Vapor Deposition) methods are used to form TiN films. The PVD method, in particular, has a treatment temperature of 500℃ or less. This allows TiN coatings to be applied to high-speed steel or die steel at or below the tempering temperature. In addition, since these hard films are made of chemical compounds they can be embed with previously unattainable characteristics such as the ability to form a very high-hardness film by shifting chemical composition ratios. Therefore, much R&D is being carried out with the aim of achieving new functional materials for coating using the PVD method. However, residual stress and strain during film formation and in use shorten the material life through film peeling and cracking. Thus it is extremely important to understand the film stress conditions.

The most effective means of measuring residual stress is X-ray diffractometry, which enables non-destructive, non-contact evaluation of crystalline materials. However, X-ray penetration depth for metals and ceramics is just a few μm, and with general-purpose measurement ($\theta/2\theta$ scanning) there are limits on selective evaluation of information only from thin films or extreme surface layers of thickness 1 μm or less. If the grazing-angle incidence method, in which X-rays are radiated only onto the sample surface, is used in this case, it is possible to control the X-ray penetration depth, and this makes it possible to evaluate residual stress in regions which can not be evaluated with a general-purpose measurement[(2)]. This section presents an example of measuring residual stress in a TiN film coated on a steel material.

2.2. Multiple-hkl method

The most widely known X-ray stress measurement method, the $\sin^2\psi$ method, is a technique that uses a specific lattice plane ($h\,k\,l$) in a polycrystalline material and observes each of the lattice spacings (d) by tilting the angle ψ. Here ψ indicates the angle between the sample surface normal and the lattice plane normal. The advantages of the $\sin^2\psi$ method are that the stress can be analyzed even if the lattice spacing (d_0) in the unstrained state is not exactly known. The stress value is easily obtained by the slope of a regression line on a graph called a $\sin^2\psi$-2θ graph, in which $\sin^2\psi$ is taken as the horizontal axis and 2θ as the vertical axis. At this time, the residual stress (σ) in the tilt of the direction of ψ angle is given as the product ($\sigma = M \cdot K$) of the regression line slope (M) and the stress constant (K) determined by the elastic constants of the material under examination.

However, a problem arises here when considering stress measurement of a thin film with the $\sin^2\psi$ method. More specifically, if the X-ray incident angle increases in order to measure the variation in lattice spacings in a single lattice plane ($h\,k\,l$), then the volume of the thin film which contributes to diffraction gets smaller. This makes it impossible to obtain sufficient diffraction intensity, and the S/N ratio from the diffraction coming from the substrate crystal worsens. To resolve this problem, a method has been proposed in which, as indicated in Fig. 1, the incident X-ray beam is introduced into the film by fixing the direction at a specific grazing-angle, and then measuring the diffraction of multiple lattice planes through 2θ scanning.

* Application Laboratories, Rigaku Corporation.
** X-ray Research Laboratory, Rigaku Corporation.

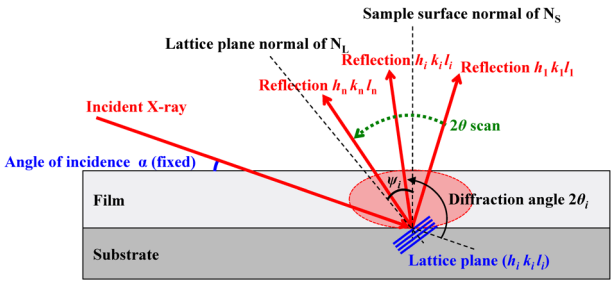

Fig. 1. X-ray stress measurement of a thin-film using the multiple-hkl method.

Since stress is analyzed using multiple lattice planes ($h_i\ k_i\ l_i$; i=1 to n), this method was later called the "multiple-hkl" method. The ψ angles of lattice planes observed through 2θ scanning are different from each other, and as a result, it is possible to observe the variation in the lattice spacings accompanying changes in the ψ angle. Therefore, this measurement method has the advantages that, for a thin film, the volume contributing to X-ray diffraction can be increased and the X-ray penetration depth can be controlled at nano nanometer scale even with thick films. The hard films presented in this section are films with fibre texture. The multiple-hkl method was applied to crystal grains with random orientation present in the film.

Equation (1) below indicates the relationship between strain and stress[3] which holds for general materials including crystalline and amorphous materials

$$\begin{aligned}\varepsilon_{\phi\psi} = {} & \frac{1}{2}S_2 \sin^2\psi[\sigma_{11}\cos^2\phi + \sigma_{12}\sin(2\phi) + \sigma_{22}\sin^2\phi] \\ & + \frac{1}{2}S_2\left[\begin{array}{l}\sigma_{13}\cos\phi\sin(2\psi) + \sigma_{23}\sin\phi\sin(2\psi) \\ + \sigma_{33}\cos^2\psi\end{array}\right] \\ & + S_1[\sigma_{11} + \sigma_{22} + \sigma_{33}] \end{aligned} \quad (1)$$

The strain $\varepsilon_{\phi\psi}$ given here indicates strain of the diffraction plane, whose surface normal is the orientation inclined by ψ in the direction rotated by ϕ in the counterclockwise direction about the surface normal of the sample. σ_{ij} (i, j=1, 2, 3) indicates the components of the stress tensor, and S_1 and $S_2/2$ are the X-ray elastic constants, represented by the Young's modulus (E) and Poisson's ratio (ν), as shown in Equation (2).

$$S_1 = -\frac{\nu}{E}, \quad \frac{1}{2}S_2 = \frac{1+\nu}{E} \quad (2)$$

With the multiple-hkl method, it is possible to analyze the stress σ_{ij} by observing the rate of change in the lattice spacing (d_i) of multiple lattice planes, i.e., the strain $\varepsilon_{\phi\psi}^{hkl}$ (=(d_i–d_{0i}/d_{0i}). At this time, d_{0i} indicates the lattice spacing in the unstrained state of the ith lattice plane.

The following equation, (3), can be derived for the equi-biaxial stress state by setting the conditions σ_{33}=0, σ_{23}=σ_{13}=σ_{12}=0, σ_{11}=σ_{22}=σ in Equation (1).

$$\begin{aligned}&\varepsilon_{\phi\psi}^{hkl} = f(\phi,\ \psi,\ S_1^{hkl},\ S_2^{hkl})\sigma, \\ &f(\phi,\ \psi,\ S_1^{hkl},\ S_2^{hkl}) \equiv 2S_1^{hkl} + \frac{1}{2}S_2^{hkl}\sin^2\psi \end{aligned} \quad (3)$$

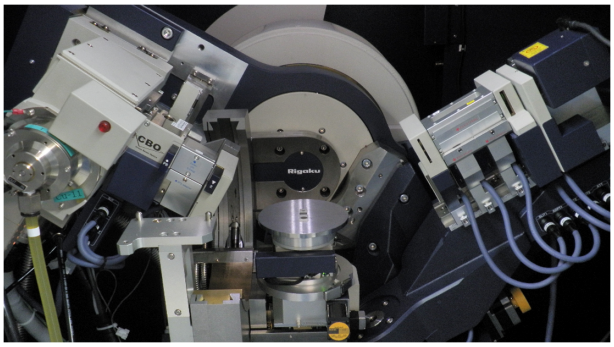

Fig. 2. SmartLab fully-automatic θ–θ rotating anode X-ray diffractometer.

If the function $f(\phi,\ \psi,\ S_1^{hkl},\ S_2^{hkl})$, based on Equation (3), is plotted on the horizontal axis and the strain $\varepsilon_{\phi\psi}^{hkl}$ on the vertical axis, then it is evident that the slope of this regression line will be the film stress σ we wish to evaluate. However, S_1^{hkl} and S_2^{hkl} show that the X-ray elastic constants depend on the lattice plane ($h\ k\ l$).

2.3. Stress measurement equipment

The SmartLab fully-automatic θ–θ rotating anode X-ray diffractometer shown in Fig. 2 was used to measure residual stress of the hard film presented in this section. A high-output (45 kV, 200 mA) rotating anode with Cu tube was used as the X-ray source, and a high-intensity parallel beam was created using a multilayer optic on the incident beam side. With a conventional optical system, a pseudo-parallel beam formed by constricting the slits on the incident side and receiving side, is limited on reduction of the angle of divergence available since flux is reduced dramatically. In contrast, if an optical element (CBO: Cross Beam Optics) with a parabolic multilayer mirror is used, it is possible to use an X-ray beam whose reflectivity of X-ray intensity is 70%, and with an angle of divergence is 0.04°. On the receiving side, divergence of the diffracted X-rays was suppressed by using a parallel slit analyzer (PSA: Parallel Slit Analyzer) with a resolution of 0.5°.

2.4. Results of measurement and analysis using the multiple-hkl method

A steel material coated with a TiN film, using an ion plating method classified as a PVD technique, was used for the measurement. The film thickness was approximately 5 μm, and the film surface had a silver luster. Incidentally, it is generally known that the color of a Ti_xN_{1-x} film varies depending on the nitrogen content, exhibiting a gold color with x=0.5 and a silver color with x=0.5. That is, it was assumed that the TiN film had a low reaction amount of nitrogen since the sample used was silver.

Figure 3 shows the diffraction profile observed through 2θ scanning with the incident X-ray angle fixed at approximately 0.4°. By comparing the intensity ratio of each reflection in the actual measured profile with the intensity ratio of each reflection in the diffraction profile for a randomly oriented sample, it was determined

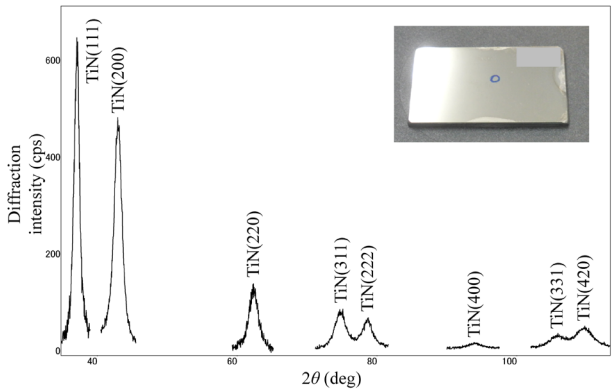

Fig. 3. Diffraction profile of a TiN film using grazing-angle incidence method.

Table 1. Diffraction peak information for TiN film.

h k l	2θ (deg)	FWHM (deg)	*I* (counts)
1 1 1	37.20	0.92	7182
2 0 0	42.93	1.35	5291
2 2 0	62.39	1.64	1505
3 1 1	74.80	1.88	883
2 2 2	78.66	1.66	654
4 0 0	94.00	2.33	130
3 3 1	105.70	2.80	232
4 2 0	109.57	2.64	449

that the sample has a weak preferred orientation in the [111] axis direction. When the incident X-ray beam was introduced at a grazing-angle, the penetration depth of X-rays into the TiN film was a few tens of nm, and thus, the stress state of the extreme surface layer is evaluated relative to the film thickness.

Here, Table 1 shows the diffraction peak information for the TiN film, obtained from profile fitting.

In the stress analysis using the multiple-hkl method, the stress value was calculated using six reflections on the high angle side (out of eight observed reflections), while taking into account strain sensitivity. Based on Equation (3), the tensile stress observed in the TiN film had values of σ=1.99 GPa for stress, and $\Delta\sigma$=0.47 GPa for the confidence limit. Figure 4 shows a graph of the function $f(\phi, \psi, S_1^{hkl}, S_2^{hkl})$ versus the strain ε_ψ^{hkl}. The values of the Young's modulus and Poisson's ratio were set to E=429 GPa, and ν=0.19, respectively, while treating the material as a homogeneous isotropic body.

2.5. Discussion

The main cause of residual stress in thin films is thought to be thermal stress, which arises due to differences in the linear expansion coefficients of the substrate and film. The linear expansion coefficients of Fe and TiN near room temperature are, respectively, 11.8×10^{-6}/K and 9.2×10^{-6}/K, and after film formation, it is thought that compressive stress remains due to thermal

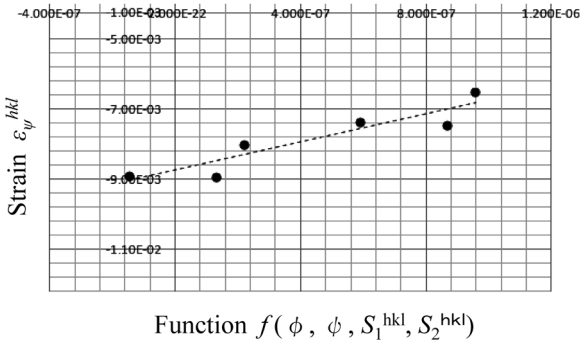

Fig. 4. Graph of function $f(\phi, \psi, S_1^{hkl}, S_2^{hkl})$ vs. strain ε_ψ^{hkl}.

contraction of the substrate. However, in the stress measurement, the residual stress of the extreme surface layer is evaluated relative to the film thickness, and it is certainly possible that the way in which strain develops is different from that near the boundary between the film and substrate. That is, while the substrate is strongly restrained near the boundary, there is a possibility that stress relaxation occurs at the film surface. In addition, a linear relationship is obviously shown in the function $f(\phi, \psi, S_1^{hkl}, S_2^{hkl})$ vs. strain ε_ψ^{hkl} graph, and thus it can be seen that the conditions used to derive Equation (3) reflect the stress state of the film, and that tensile stress remains in the film surface in an isotropic state. If an anisotropic stress state needs to be taken into account, the stress can be analyzed by setting $\sigma_{11}\neq\sigma_{22}$ and $\sigma_{12}\neq0$ in Equation (1). In addition, the linearity of the observed graph shows that the stress gradient has no effect within the X-ray penetration depth.

2.6. Review of the multiple-hkl method

Another advantage of the multiple-hkl method is that it can be applied to stress measurements in narrow areas. At measurement points with fixing the X-ray angle of incidence, such as those in the narrow bottoms between gear teeth or in the inside of wheels, the stress is facilitated to be measured by taking into account only the X-ray angle of diffraction.

For the above reason, the multiple-hkl method is effective for evaluating residual stress in thin films and narrow areas, and it is an analysis technique indispensible for complementing general-purpose methods of X-ray measurement.

3. Evaluation of residual stress in a sample with shear stress in the depth direction

3.1. Comparison with the conventional method of residual stress measurement

If the $\sin^2\psi$ method, which is a uniaxial stress measurement method, is used with a polycrystalline sample, the sample must satisfy the following four conditions.

① Sufficient crystal grains are present in the area irradiated by X-ray.
② No strong texture is present in a sample.

③ Stress induced in a sample is bi-axial (σ_{33}=σ_{23}=σ_{13}=0).
④ No stress gradient is present within the X-ray penetration depth.

Since the above four preconditions exist with the $\sin^2\psi$ method, depending on the sample's crystal state, the $\sin^2\psi$–2θ graph may display large deviations or may bend and become non-linear. The cause of this is thought to be the following four crystal states given by ①′ to ④′ below, which correspond to the above ① to ④, respectively.

①′ Coarse crystal grains have been formed, thus a sufficient number of crystal grains are not present within the X-ray irradiated area.
②′ Texture is present.
③′ Shear stress component (σ_{13} or σ_{23}) is present within the X-ray penetration depth.
④′ Steep stress gradient is present within the X-ray penetration depth.

In addition, it is known, by taking into account the triaxial stress state for the above crystal states, that the four features indicated in the following ①″ to ④″ appear in the $\sin^2\psi$–2θ graph, corresponding to the above ①′ to ④′, respectively.

①″ A continuous profile is not observed, and thus there is a large error in the slope of the $\sin^2\psi$–2θ graph.
②″ Peak intensities of the profiles observed with ψ in specific directions are remarkably low.
③″ ψ split is produced[4),(5)].
④″ Waving appears in the $\sin^2\psi$–2θ graph.

Various residual stress measurement and analysis techniques have previously been proposed for samples with crystal states outside the scope of application of the $\sin^2\psi$ method. However, even if phenomena like those indicated here appear in the $\sin^2\psi$–2θ graph, it is a well-known fact that the $\sin^2\psi$ method can still be used if the confidence limit (an indicator of the match between the $\sin^2\psi$–2θ graph and the regression line) does not become large.

This section considers the crystal state that produces a ψ split. If the shapes differ between two $\sin^2\psi$–2θ graphs observed in the $+\psi$ and $-\psi$ directions which differ by 180° in the direction in which stress is measured, and the slopes of the regression lines of the two $\sin^2\psi$–2θ graphs differ in the $+\psi$ and $-\psi$ directions, then the respective observed stress values will also differ from each other. If, at this time, stress is only evaluated on one side using the conventional $\sin^2\psi$ method, a large discrepancy may arise between the evaluated and actual stress values.

Therefore, the following section will present a method of residual stress evaluation for the ψ split which is a problem when using the $\sin^2\psi$ method, and this will be called the ψ split method. However, a laboratory X-ray source was used here, and thus the stress in the depth direction was set to 0 (σ_{33}=0).

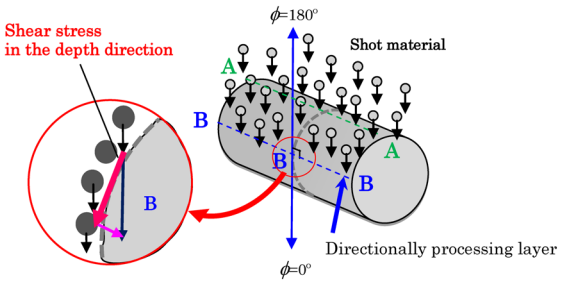

Fig. 5. Shear stress applied due to shot peening.

3.2. Theory and technique evaluating residual stress with ψ split

When evaluating residual stress for a certain material, typical samples which might contain a shear stress component (σ_{12} or σ_{23}) are those in which a directionally processing layer is formed using techniques such as cutting or grinding. This section discusses the method of evaluating residual stress when a ψ split occurs, using as an example a sample with a directionally processed layer formed through shot peening treated from one direction only.

When residual stress parallel to the in-plane component of the force (red arrow mark) is evaluated using the $\sin^2\psi$ method in the directionally processing layer (on the B line) as shown in Fig. 5, it is known that the $\sin^2\psi$–2θ graphs in the two directions observed for the $+\psi$ and $-\psi$ directions are divided into the top and bottom of an ellipse. Hereafter, the $+\psi$ direction will be indicated as ψ_+ and the $-\psi$ direction as ψ_-. The X-ray residual stress was evaluated for a sample for which a ψ split was intentionally produced by treating shot peening from one direction on a round iron rod.

The close-up view in Fig. 5 shows the stress component added to the round rod by the shot, viewing from the rod's cross section. Relative to the positions A and B in the circumferential direction where the shot contacts the round rod, the shot strikes the sample surface perpendicularly at A. At B, on the other hand, the shot strikes in a "shearing" fashion from an inclined direction, and thus at B a stress (strain) component parallel to the sample surface, i.e., a shear stress component, is produced, and a directionally processing layer is formed.

Figure 6 shows the triaxial stress state in the directionally processing layer B. If the direction of incidence of the shot is taken to be parallel to the σ_1–σ_3 plane, then there is a shear stress component σ_{13} in the depth direction, and thus the σ_3 axis will tilt from the surface normal of the sample (σ_{33} axis direction) due to rotation of the principal stress axes (red arrow; the three normal stress components when the shear stress components in all directions become zero are called the principal stress) around the σ_2 axis.

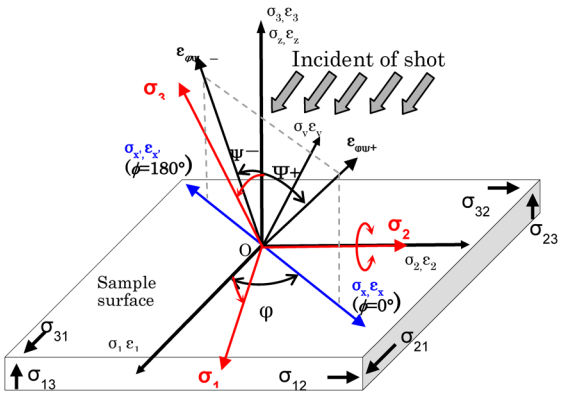

Fig. 6. Triaxial stress state at position B.

In addition, the relationship between strain and stress in the sample coordinate system is given by the following Equation (4)[12] due to the assumption here that σ_{33} is set equal to zero in the general Equation (1) which indicates the state of triaxial stress[12].

$$\varepsilon_{\phi\psi}=\frac{1}{2}S_2(\sigma_{11}\cos^2\phi+\sigma_{12}\sin 2\phi+\sigma_{22}\sin^2\phi)\sin^2\psi +S_1(\sigma_{11}+\sigma_{22})+\frac{1}{2}S_2(\sigma_{13}\cos\phi+\sigma_{23}\sin\phi)\sin 2\psi \quad (4)$$

For Equation (4), the strain $\varepsilon_{\phi+\psi}$ and $\varepsilon_{\phi-\psi}$ in the ψ_+ and ψ_- directions with respect to ϕ correspond, respectively, to the strain $\varepsilon_{\phi\psi}$ and $\varepsilon_{\phi+180°\psi}$ of ψ with respect to ϕ and ϕ+180°. Therefore, the following Equation (5) is obtained if the average of these strains $(\varepsilon_{0°\psi}+\varepsilon_{180°\psi})/2$ (setting ϕ=0°) is calculated using Equation (4).

$$\frac{1}{2}(\varepsilon_{0°\psi}+\varepsilon_{180°\psi}) =\frac{1}{2}S_2\sigma_{11}\sin^2\psi+S_1(\sigma_{11}+\sigma_{22}) \quad (5)$$

In addition, strain at the crystal plane in the X-ray diffraction method is expressed as $\varepsilon_{\phi\psi}=(d-d_0)/d_0$, and thus $\varepsilon_{\phi\psi}=(\sin\theta_0/\sin\theta)-1$ is obtained using Bragg's equation $2d\sin\theta=n\lambda$ (n=1). Therefore, if the diffraction angle 2θ in the ψ_+ direction is indicated as $2\theta_+$, and the diffraction angle 2θ in the ψ_- direction as $2\theta_-$, and if 2θ is partially differentiated by $\sin^2\psi$ in Equation (5), and the result is rewritten using $S_2/2(1+\nu)/E$, the following Equation (6) is obtained:

$$-(\partial 2\theta_+ + \partial 2\theta_-)\cot\theta_0/2=\frac{2(1+\nu)}{E}\sigma\,\partial\sin^2\psi \quad (6)$$

where $\sigma=\sigma_{11}$. If M_+ and M_- are taken to be, respectively, the slopes of the $\sin^2\psi-2\theta$ graphs obtained when the sample is treated using the $\sin^2\psi$ method for the ψ_+ and ψ_- directions, and if the stress constant is assumed to be K, then the stress σ can be given finally by the following equation.

$$\sigma=-\frac{E}{2(1+\nu)}\cot\theta_0\cdot\frac{\pi}{180}\cdot\left(\frac{\partial 2\theta_+}{\partial\sin^2\psi}+\frac{\partial 2\theta_-}{\partial\sin^2\psi}\right)/2 \equiv K\cdot(M_+ + M_-)/2 \quad (7)$$

$$\begin{cases} K=-\dfrac{E}{2(1+\nu)}\cot\theta_0\cdot\dfrac{\pi}{180} & (8)\\ M_+=\dfrac{\partial 2\theta_+}{\partial\sin^2\psi} & (9)\\ M_-=\dfrac{\partial 2\theta_-}{\partial\sin^2\psi} & (10)\end{cases}$$

In other words, this indicates that the stress given by Equation (7) is equal to the average, σ_{ave}, of the residual stress values for $\sigma_{0°\psi}$ and $\sigma_{180°\psi}$ when the ψ_+ and ψ_- directions are respectively treated using the $\sin^2\psi$ method.

If it is assumed here that the confidence limits, $\Delta\sigma_{0°\psi}$ and $\Delta\sigma_{180°\psi}$, corresponding to the stress values, $\sigma_{0°\psi}$ and $\sigma_{180°\psi}$, are evaluated for the ψ_+ and ψ_- directions, respectively, then the stress values evaluated using the $\sin^2\psi$ method are given as follows:

$$\sigma_{0°\psi}\pm\Delta\sigma_{0°\psi}=K(M_+\pm\Delta M_+),\quad \sigma_{180°\psi}\pm\Delta\sigma_{180°\psi}=K(M_-\pm\Delta M_-) \quad (11)$$

where ΔM_+ and ΔM_- indicate the errors of the respective slopes M_+ and M_- of the $\sin^2\psi-2\theta$ graphs for the ψ_+ and ψ_- directions.

Therefore, the stress, σ_{ave}, obtained using the ψ split method and its error $\Delta\sigma_{ave}$ are given by the following Equation (12) by taking the respective averages using $\sigma_{0°\psi}$, $\sigma_{180°\psi}$, $\Delta\sigma_{0°\psi}$, and $\Delta\sigma_{180°\psi}$, evaluated with the $\sin^2\psi$ method.

$$\sigma_{ave}=\frac{\sigma_{180°\psi}+\sigma_{0°\psi}}{2},\quad \Delta\sigma_{ave}=\frac{\sqrt{\Delta\sigma_{0°\psi}^2+\Delta\sigma_{180°\psi}^2}}{2} \quad (12)$$

Accordingly, residual stress can be easily evaluated, with samples when ψ split occurs, by evaluating the average of the stress values in the ψ_+ and ψ_- directions using the $\sin^2\psi$ method.

3.3. Introduction of a sample measurement

The SmartLab, fully-automatic θ–θ rotating anode X-ray diffractometer (Fig. 2), was utilized to measure X-ray residual stress, and the residual stress was evaluated using the iso-inclination method in a parallel beam method optical system. Table 2 shows the measurement conditions, and Table 3 the parameters used for the analysis.

For the stress measurement, the residual stress was measured at a point on B in the two directions as shown in Fig. 5: the shot direction ψ_+ (ϕ=0°) and the opposite direction ψ_- (ϕ=180°). Figure 7 shows these two directions of stress measurements with the sample placed on the sample stage of the SmartLab.

Figure 8 shows the $\sin^2\psi-2\theta$ graph observed with the $\sin^2\psi$ method for the ψ_+ (ϕ=0°) and the ψ_- (ϕ=180°) directions.

At one measurement point on B, compressive stress was observed at both ψ=0° and ψ=180°, but a typical ψ split was observed in which the $\sin^2\psi-2\theta$ graphs are curved and the respective stress values are

Table 2. Measurement conditions.

Characteristic X-rays	CuKα
Diffraction surface	α-Fe (3 1 0)
Strain-free diffraction angle	$2\theta_0$=116.38°
Measurement method	Constant ψ method (iso-inclination method)

Table 3. Analysis conditions.

Analysis technique	$\sin^2\psi$ method
Young's modulus	223300 MPa
Poisson's ratio	0.28
Stress constant	−941.53 MPa/°

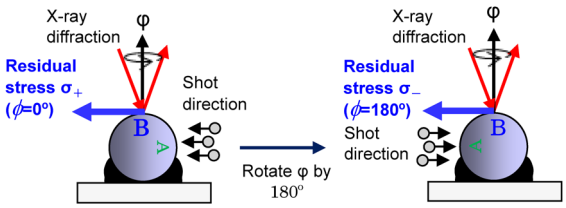

Fig. 7. Stress measurement directions at a measurement point on B viewing from the cross-section side of the round rod.

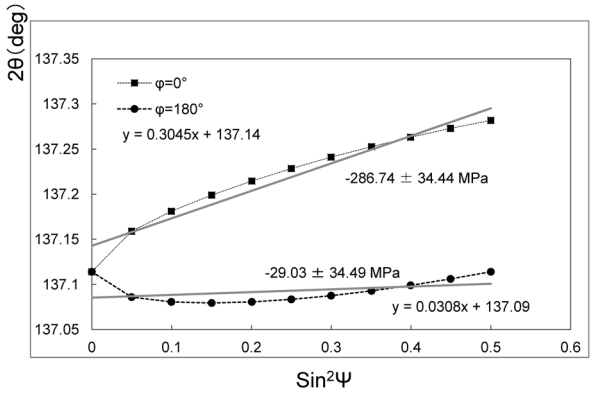

Fig. 8. $\sin^2\psi$−2θ graph in working directions (ϕ=0°, ϕ=180°) of shot peening at a measurement point on B. (Sample provided by: Professor Shinichi Oya, Tokyo City University)

different from each other. The residual stress value in the ϕ=0° direction at a measurement point on B was −286.74±34.44 MPa, and the residual stress value in the ϕ=180° direction was −29.03±34.49 MPa. Thus, the residual stress value at the measurement point where the ψ split occurred was calculated to be −157.89±24.37 MPa by taking the average value based on the ψ split method.

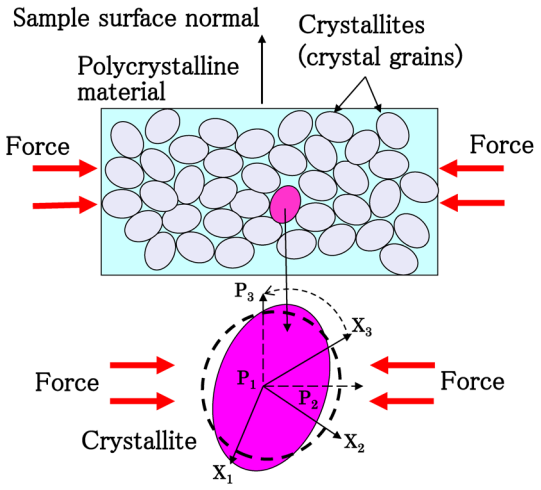

Fig. 9. A polycrystalline material consisting of numerous crystallites (crystal grains). Each crystallite has its own coordinate system.

4 Residual stress measurement and line-broadering of diffraction in a sample with fibre texture using the crystallite strain analysis method

4.1 Residual stress measurement using the crystallite strain analysis method

This is a technique for analyzing residual stress from crystallites comprising a polycrystalline material. In Europe, this technique is generally known as the crystallite group method (CGM)[6]. Since this analysis method determines the strain of the entire crystal from a point of view of the orientation and strain of the crystallites comprising the polycrystalline material, we call this technique the "crystallite strain analysis method." This section discusses a technique for applying the crystallite strain analysis method to polycrystalline materials with fibre texture. Developments of this measurement method for films with fibre texture was proposed by Hanabusa[7] for the hexagonal system, and since then analysis techniques for biaxial and triaxial stress states have been proposed by Sasaki[8], Ejiri[8], Tanaka[9] and others. Recently, Yokoyama et al.[1] have developed formulae indicating the relationships between strain and stress, obtained by taking account of the symmetries of a single crystal to which the constituent crystallites belong. In addition, when crystallite strain in samples with fibre texture is taken into account, it has also turned out that line-broadening is observed from the crystallite symmetries[10]. This line-broadening will also be discussed.

In Fig. 9, focusing on one crystallite in a polycrystalline material, the sample coordinate system $\mathbf{P}_i$ for the stress measurement is taken into account. When the crystallite under measurement is shown by the crystal coordinate system $\mathbf{X}_i$ in the sample, the laboratory coordinate system, in which strain of lattice planes is measured, is taken to be $\mathbf{L}_i$, as shown in Fig. 10.

The direction in which stain of a lattice plane is

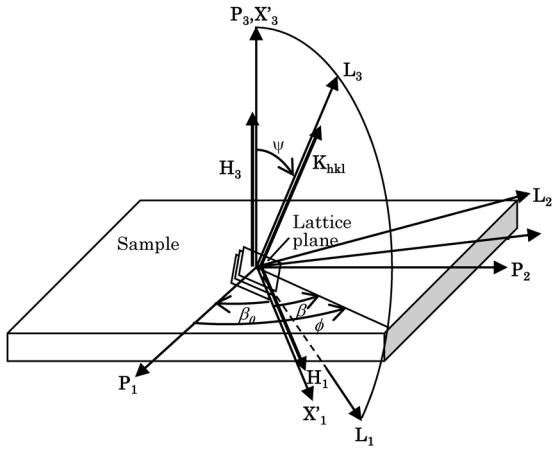

Fig. 10. The four coordinate systems, $\mathbf{X}'_i$, $\mathbf{P}_i$, L_i, and $\mathbf{X}_i$, in a polycrystalline material. $\mathbf{K}_{hkl}$ indicates a scattering vector in the $\mathbf{L}_3$ direction.

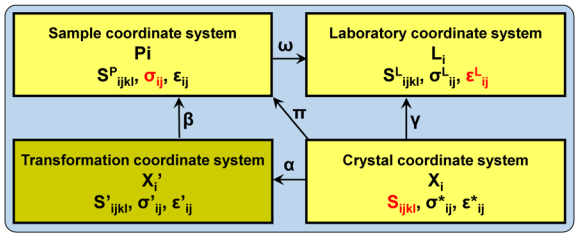

Fig. 11. The four coordinate systems transformable from one to another using the matrices (α, β, π, ω, γ). $\mathbf{X}'$ indicates a coordinate system added for convenience.

measured is taken to be the L_3 axis direction.

Figure 11 shows the relationship between the three (or four) coordinate systems, which are referred to in the stress analysis of a polycrystalline material as indicated above.

The four coordinate systems can be transformed to one another using the five matrices α, β, π, ω and γ. Strain and stress are expressed with a second order tensor, and thus if the strain $\varepsilon^{\mathrm{L}}_{33}$ in the L_3 axis direction observed with X-rays is indicated by the stress σ_{kl} of the sample coordinate system, then $\varepsilon^{\mathrm{L}}_{33}$ can be found using Equations (13) to (16).

$$\varepsilon_{ij} = S^P_{ijkl}\,\sigma_{kl} \tag{13}$$

$$S^P_{ijkl} = \pi_{ip}\,\pi_{jq}\,\pi_{kr}\,\pi_{ls}\,S_{pqrs} \tag{14}$$

$$\varepsilon^L_{33} = \omega_{3i}\,\omega_{3j}\,\varepsilon_{ij} \tag{15}$$

$$\varepsilon^L_{33} = \omega_{3i}\,\omega_{3j}\,S^P_{ijkl}\,\sigma_{kl} \tag{16}$$

In other words, $\varepsilon^{\mathrm{L}}_{33}$ is the strain derived from the relationship between the strain and stress in the single crystal of a constituent crystallite in a polycrystalline material.

In this stress analysis, it is treated that the stress of each crystallite in a polycrystalline material with fibre texture is equal to the macro stress based on the Reuss model. The average stress in the polycrystalline material $\langle\varepsilon^{\mathrm{L}}_{33}\rangle$ is given by the following equation.

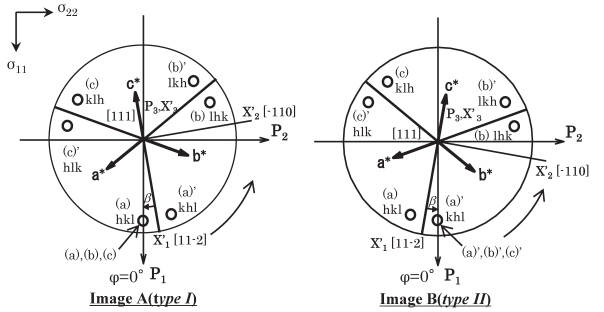

Fig. 12. Orientations of two crystallites, type I and type II, in a sample having fibre texture of $\langle 111\rangle$ axis and belonging to cubic system.

$$\begin{aligned}\left\langle \varepsilon^L_{33}\right\rangle &= \left\langle \omega_{3i}\,\omega_{3j}\,S^P_{ijkl}\,\sigma_{kl}\right\rangle \\ &= \left\langle \omega_{3i}\,\omega_{3j}\,S^P_{ijkl}\right\rangle \sigma_{kl}\end{aligned} \tag{17}$$

In the Reuss model, since the stress is equal to the average stress (macro stress) of the sample, the stress σ_{kl} can be expressed on the outside of the angular parentheses $\langle\ \rangle$ in Equation (17).

Figure 12 shows a stereographic projection in the $\langle 111\rangle$ axis direction when the constituent crystallites of a sample, having the $\langle 111\rangle$ axis as the fibre texture, belong to the cubic system with m-3 m for the Laue symmetry. Based on the symmetries in a single crystal of the crystallite, each crystallite has three mirror planes containing the $\langle 111\rangle$ axis and the reciprocal lattice axes a^*, b^* and c^*, respectively, so that there are six equivalent reflections around the $\langle 111\rangle$ axis. When taking these six equivalent reflections to be (a), (a)′, (b), (b)′, (c) and (c)′, both groups of the three reflections (a), (b), (c) and the three reflection (a)′, (b)′, (c)′ have a relationship of 120° rotational symmetry, and the corresponding reflections such as (a) and (a)′ have a mirror plane between them.

Since the sample has the $\langle 111\rangle$ axis as the fibre texture, it is likely that numerous crystallites are arranged at random around the $\langle 111\rangle$ axis. That is, the position (a) of a certain crystallite is overlapped by equivalent reflections (a)′, (b)′, ..., (c)′ of other crystallites. However, generally there is no way to distinguish the overlapping reflections of multiple crystallites such as (a), (b), (c) and (a)′, (b)′, (c)′.

Next, let us consider the relationships between the symmetries in a single crystal and its residual stress. As shown in Fig. 12, when strain is observed at ϕ=0°, the positions (a), (b), (c) and (a)′, (b)′, (c)′, which have the 120° rotational symmetry and are equivalent, cannot be distinguished, so that it is enough if one point from each group is taken as a representative point that the residual stress should be taken into account only for (a) and (a)′. These two representatives are shown as type I and type II in Fig. 12. If $\varepsilon^{\mathrm{L}}_{33\mathrm{I}}$ and $\varepsilon^{\mathrm{L}}_{33\mathrm{II}}$ indicate, respectively, two strains observed when the diffraction conditions are satisfied in type I and type II, and the biaxial stress state is assumed, then $\varepsilon^{\mathrm{L}}_{33\mathrm{I}}$ and $\varepsilon^{\mathrm{L}}_{33\mathrm{II}}$ are calculated as follows from Equation (16):

$$\varepsilon_{33I}^{L} = \frac{1}{12}\{(3s_{44}+3s_{44}\cos 2\phi+2s_0\cos 2\phi)\sin^2\psi - 2\sqrt{2}s_0\cos(3\beta-2\phi)\sin 2\psi+12s_{12}+4s_0\}\sigma_{11} + \frac{1}{12}\{(3s_{44}-3s_{44}\cos 2\phi-2s_0\cos 2\phi)\sin^2\psi + 2\sqrt{2}s_0\cos(3\beta-2\phi)\sin 2\psi+12s_{12}+4s_0\}\sigma_{22} + \frac{1}{6}\{(3s_{44}+2s_0)\sin 2\phi\sin^2\psi + 2\sqrt{2}s_0\sin(3\beta-2\phi)\sin 2\psi\}\sigma_{12} \quad (18)$$

$$\varepsilon_{33II}^{L} = \frac{1}{12}\{(3s_{44}+3s_{44}\cos 2\phi+2s_0\cos 2\phi)\sin^2\psi - 2\sqrt{2}s_0\cos(3\beta+2\phi)\sin 2\psi+12s_{12}+4s_0\}\sigma_{11} + \frac{1}{12}\{(3s_{44}-3s_{44}\cos 2\phi-2s_0\cos 2\phi)\sin^2\psi + 2\sqrt{2}s_0\cos(3\beta+2\phi)\sin 2\psi+12s_{12}+4s_0\}\sigma_{22} + \frac{1}{6}\{(3s_{44}+2s_0)\sin 2\phi\sin^2\psi - 2\sqrt{2}s_0\sin(3\beta+2\phi)\sin 2\psi\}\sigma_{12} \quad (19)$$

where σ_{11}, σ_{22} and σ_{12} are the stress components in the sample coordinate system, ϕ and ψ observed orientations of ε_{33}^{L} shown in Fig. 10, and β the angle from the mirror plane to (a) or (a)′, as indicated in Fig. 12. In addition, when s_{11}, s_{12} and s_{44} indicate the elastic compliance constants of a single crystal in cubic system, then $s_0=s_{11}-s_{12}-s_{44}/2$. Here, the following equations show the relationships ψ and β have to the scattering vector $\mathbf{K}_{hkl}$ and the vectors $\mathbf{H}_1$ and $\mathbf{H}_3$ shown in Fig. 10.

$$\psi = \cos^{-1}\left(\frac{\mathbf{H}_3\cdot\mathbf{K}_{hkl}}{|\mathbf{H}_3||\mathbf{K}_{hkl}|}\right), \quad (20)$$

$$\beta = \cos^{-1}\left(\frac{(\mathbf{K}_{hkl}\times\mathbf{H}_3)\cdot(\mathbf{H}_1\times\mathbf{H}_3)}{|\mathbf{K}_{hkl}\times\mathbf{H}_3||\mathbf{H}_1\times\mathbf{H}_3|}\right) \quad (21)$$

It is predicted that the two types of strains, which differ from each other in a stress state of the sample, will be observed simultaneously at the same point (ϕ=0°). This is attributable to the fact that the crystallinity of the sample with fibre texture displays a rocking curve ≤0.1°, and that the X-ray source for measurement has some angular divergence and some wavelength dispersion. Therefore, the strains of the respective crystallographic planes in the type I and type II differ from each other. However in the observed diffractions, it is expected that the respective diffraction lines observed will overlap each other and form a single peak.

In the Reuss model, the observed strain, i.e., the average strain of the sample $\langle\varepsilon_{33}^{L}\rangle$ is calculated as follows as the average of the strains ε_{33I}^{L} and ε_{33II}^{L} for type I and type II.

$$\left\langle\varepsilon_{33}^{L}\right\rangle = \frac{1}{12}\{(3s_{44}+3s_{44}\cos 2\phi+2s_0\cos 2\phi)\sin^2\psi - 2\sqrt{2}s_0\cos(3\beta-2\phi)\sin 2\psi+12s_{12}+4s_0\}\sigma_{11} + \frac{1}{12}\{(3s_{44}-3s_{44}\cos 2\phi-2s_0\cos 2\phi)\sin^2\psi + 2\sqrt{2}s_0\cos(3\beta-2\phi)\sin 2\psi+12s_{12}+4s_0\}\sigma_{22} + \frac{1}{6}\{(3s_{44}+2s_0)\sin 2\phi\sin^2\psi + 2\sqrt{2}s_0\sin(3\beta-2\phi)\sin 2\psi\}\sigma_{12} \quad (22)$$

In general, stress is obtained from data consisting of strain observed at several points by applying the method of least squares refinement to Equation (22). In this paper, the relationship between strain and stress in the constituent crystallites was evaluated by assuming a biaxial stress state, however relationship for a triaxial stress state can also be estimated in the same way from Equation (16).

4.2. Line-broadening of diffraction in the crystallite strain analysis method

If two strains observed at the type I and type II orientations, respectively, of the constituent crystallites in a sample with fibre texture are different from each other, as expected in the previous section, it is predicted that line-broadening[12] of the diffraction will be observed.

Thus, the line-broadening of the diffraction, $\Delta 2\theta(\beta, \phi, \psi)$, is estimated as follows, where the difference of stains in Equations (18) and (19) is indicated as $\Delta\varepsilon_{33,II-I}^{L}$.

$$\Delta 2\theta(\beta,\phi,\psi) = |\delta 2\theta(I) - \delta 2\theta(II)| = |-2\tan(\theta_0)\Delta\varepsilon_{33,II-I}^{L}| \quad (23)$$

The following equation shows the results of calculating the strain difference $\Delta\varepsilon_{33II-I}^{L}$ which is the cause of the line- broadening of diffraction of a sample with ⟨111⟩ fibre texture in a cubic system.

$$\Delta\varepsilon_{33II-I}^{L} = \varepsilon_{33,II}^{L}(\beta,\phi,\psi) - \varepsilon_{33,I}^{L}(\beta,\phi,\psi) = -\frac{1}{3}\sqrt{2}s_0\sin 3\beta\{(\sigma_{22}-\sigma_{11})\sin 2\psi\sin 2\phi + 2\sigma_{12}\sin 2\psi\cos 2\phi + 2(\sigma_{23}\cos\phi-\sigma_{13}\sin\phi)\sin^2\psi\} \quad (24)$$

Equation (24) shows that, when the difference of the normal stress components (difference of σ_{11} and σ_{22}) is large, i.e., in an anisotropic stress state, there is a tendency for a large amount of line-broadening in diffraction to appear in the ϕ=45° direction. On the other hand, there is tendency for a large amount of the shear stress components σ_{12} and σ_{23} to appear in the ϕ=0° direction.

5. Conclusion

The three examples of X-ray stress analysis methods presented here are not frequently discussed as ordinary

analysis methods, but they are practical and effective stress analysis methods. Quantification of residual stress can serve as an indicator of material and structure strength, and thus it is an important issue for evaluating materials. Some of the techniques shown here have been commercialized by Rigaku in Japan.

References

(1) R. Yokoyama and J. Harada . *J. Appl. Cryst.,* **42** (2009), 185−191.

(2) C. H. Ma, J. H. Huang and H. Chen: *Thin Solid Films*, **418** (2002), 73−78.

(3) U. Welzel, J. Ligot, P. Lamparter, A. C. Vermeulen and E. J. Mittemeijer: *J. Appl. Cryst.*, **38** (2005), 1−29.

(4) T. Hanabusa and H. Fujiwara: *J. Soc. Mater. Sci. Jpn.*, **30** (1981), 1095−1101.

(5) T. Hanabusa and H. Fujiwara: *J. Soc. Mater. Sci. Jpn.*, **31** (1982), 227−233.

(6) U. Welzel and E. J. Mittemeijer: *Mater. Sci. Forum*, **443–444** (2004), 131−134.

(7) T. Hanabusa: *J. Soc. Mater. Sci. Res. Int.*, **5** (1999), 63−73.

(8) S. Ejiri, Z. Lin, T. Sasaki and Y. Hirose: *J. Soc. Mater. Sci. Jpn.*, **46** (1997), 750−755.

(9) K. Tanaka, Y. Akiniwa, T. Ito and K. Inoue: *Jpn. Soc. Mech. Eng. Int. J.*, *Ser. A*, **42** (1999), 224−234.

(10) R. Yokoyama, J. Harada and Y. Akiniwa: *J. Appl. Cryst.,* **42** (2009), 776−782.